The EMPIR initiative is co-funded by the European Union's Horizon 2020 research and innovation programme and the EMPIR Participating States

Calibration of power sensors for low-power measurement

Document Type: Best practice guide

Authors: Manuel Rodríguez[1], Murat Celep[2], Martin Hudlicka[3], Abdel Rahman Sallam[4], George Krikelas[5], Borut Pinter[6], Łukasz Usydus[7]

Activity Partners: INTA[1], TUBITAK UME[2], CMI[3], NIS[4], EIM/NQIS[5], SIQ[6], GUM[7]

May 2019

CONTENTS

1. Introduction

Basically two techniques can be considered when trying to characterize power sensors: those measurement techniques based on temperature-stabilized thermistor mounts (feedthroughs, see Ref. [8] and Ref. [9]) and those based on the use of common power sensors (thermocouples) of the same type as the unit under test. The latter technique is commonly known as direct comparison transfer, DCT, or simply the two- or three-sensor method, depending on the number of power sensors involved.

The measurement method based on temperature-stabilized thermistors requires the purchase, maintenance and periodic calibration of this type of mounts, commonly known as feedthroughs, which in essence are capable of generating a known amount of power at the reference plane. Also some additional instrumentation, such as the control unit, is required, and the overall investment in the acquisition of measurement equipment and in the training of specialized staff is considerable. Besides, different feedthroughs have to be maintained for each connector type, and not all RF connectors are commercially available, except for the most common ones, Type N and PC 3.5 mm.

On the other hand, the direct comparison transfer (DCT) for characterization of power sensors is based on the comparison of the sensor under test against another piece of equipment which has been previously characterized (calibrated) and normally has similar characteristics. In the case of power sensor for low-power measurement (diode type power sensor), see Fig. 1, it is not strictly necessary to have a calibrated diode type power sensor (diode sensor), use can be made of a mid-power thermocouple and a calibrated attenuator for reduction of incoming power to the unit under test. This method has the advantage that all involved reflection coefficients are known in magnitude and phase, which allows us to correct for impedance mismatch making use of complex (vector) formulas. This is difficult to achieve in the case of temperature-stabilized thermistor mounts, since the only way to gain knowledge about the complex reflection coefficient of a feedthrough is to disassemble the internal power splitter (in occasions it is necessary to remove the housing) and to separately characterize it with a VNA.

Mismatch correction reduces overall uncertainty. Since we are correcting for impedance mismatch, only the uncertainties with which the reflection coefficients are known are to be incorporated into the uncertainty budget. Whereas in the case of no correction, it is the magnitude of the involved reflection coefficient which has to be accounted for, hence making the mismatch contribution higher.

Partial differentiation of the complex formulas that give us the mismatch correction as a function of all involved complex reflection coefficients (known in terms of magnitude and phase, or equivalently in real and imaginary part) is not straightforward. The Monte Carlo (MC) method allows us to avoid this mathematical difficulty, i.e. to solve for the sensitivity of the scalar mismatch correction with respect to the real and imaginary parts of all reflection coefficients, including also the complex scattering [S] parameters of the padding attenuator in case it may be needed in calibration of diode power sensors.

Fig. 1. An example of power sensor for low-power measurement (diode type power sensor).

In this guide, we will mainly focus on the most common measurement configuration of three sensors (one leveling sensor, the standard or calibrated sensor and the sensor under test). As first approach, we assume that a calibrated diode sensor is available at the laboratory. Later on, we will introduce also the correction of a padding attenuator with which the power level incident onto the diode sensor under test is reduced: by doing this, we can compare between a diode sensor under test and a calibrated mid-power thermocouple.

2. Overview of available measurement methods

As said in the introduction, the characterization of power sensors is traditionally based on the comparison against standard thermistor mounts, stabilized in temperature and commonly known as feedthroughs. These mounts, together with the associated instrumentation (namely a control unit, see Fig. 2) act as a known power generator: the reading of the sensor element serves as feedback to the control unit in such a way that a constant power level is maintained at the output port of the embedded power splitter. Calibration of the feedthrough consists in determining this output power at the different working frequencies, through the measured calibration factor of the standard mount. Calibration is made by comparison against a known, temperature-stabilized terminating mount plus a Type IV dual voltmeter, but it is not the purpose of this best practice guide to explain in detail the characterization of thermistor mounts.

In short, with this type of instrumentation the laboratory has to assure traceability of the standard feedthrough used to calibrate common thermocouples and diode sensors. This can be made either by sending the feedthrough unit or by sending the terminating thermistor which in turn will provide traceability to the feedthrough. As can be easily understood, use of these types of standards, apart from their intrinsic acquisition cost, requires additional instrumentation, additional training for its usage which is not trivial, and requires of course periodic calibration whose cost is usually higher as compared with a common thermocouple or diode sensor.

On the other hand, the lack of knowledge about the complex reflection coefficient of the working standard in magnitude and phase means that it is not possible to correct for impedance mismatch. Even the determination of magnitude of this reflection coefficient requires the use of the ripple technique which is not straightforward (unless the internal power splitter is extracted from its housing and characterized apart). If the mismatch correction is not applied to the measured calibration factor of the device under test (thermocouple or diode), this term has to be incorporated into the uncertainty budget, normally in the form of maximum bound for its contribution (e.g. $200 \cdot |\Gamma_{Std}| \cdot |\Gamma_{DUT}|$ in percent).

Fig. 2. Temperature-stabilized feedthrough mount (left) and control unit (right)

The direct comparison transfer is based on the comparison of the sensor under test against a calibrated thermocouple of similar characteristics with the aid of a power splitter,

see Fig. 3. Besides, the same standard mid-power sensor can be used for calibration of mid- and low-power sensors, since the level of power incident onto the sensor under test can be reduced with the aid of a padding attenuator. The calibrated power sensor acts as the traveling standard, therefore it can be sent for calibration to an external laboratory. The only drawback of the method is the worse long-term stability characteristics that common thermocouples exhibit as compared with thermistor mounts stabilized in temperature. However, the simplicity of the measurement setup and the affordability of the associated instrumentation compensates for this drawback.

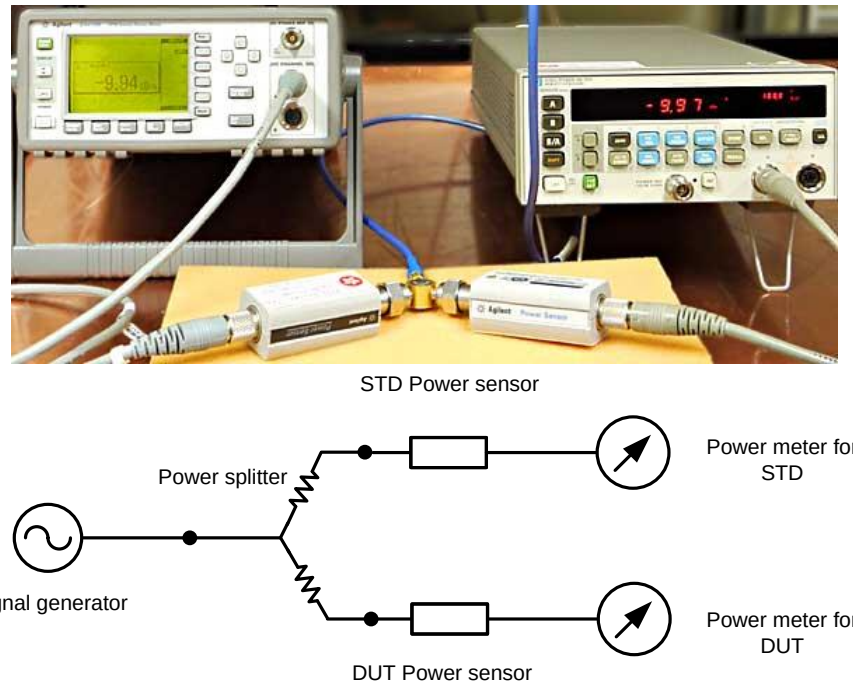

Fig. 3. Direct comparison transfer: measurement setup and schematic representation (two-sensors)

Strongest point of the direct comparison transfer is that all reflection coefficients can be known in magnitude and phase, which allows us to correct for impedance mismatch. This reduces the mismatch contribution to uncertainty, since it is only necessary to account for the uncertainties with which the reflection coefficients (real and imaginary, or magnitude and phase) are known. These uncertainties are propagated through the Law of Propagation of Uncertainties (LPU) onto the scalar correction which is to be applied to the measured calibration factor of the unit under test.

The Monte Carlo (MC) method allows us to avoid performing the LPU with three, or even six to seven complex variables, which would require partial differentiation with respect to the real and imaginary part of each of them. In the two-sensors configuration, four reflection coefficients would be involved, those of the standard sensor and of the sensor under test, and the equivalent source match of the power splitter in both output ports, plus the complex tracking between splitter arms. As a second example, moving onto a configuration with three power sensors (including a third one for leveling), there are three reflection coefficients involved: that of the DUT, that of the standard and the equivalent source match in one of the splitter output ports. Another example: if translation of the reference plane of the sensor is required to correct for the [S] parameters of an attenuator or adapter (in order to reduce the level of power that reaches the diode sensor with respect to the incoming power onto a mid-power standard, or simply to adapt their respective connector types to the same splitter output), this would require the knowledge of four complex [S] parameters plus the reflection coefficients of both sensors and the equivalent source match of the splitter. The use of MC against the analytical solution via the LPU is more and more advisable as the number of involved parameters increase.

In the examples shown in this guide, simulations made by Monte Carlo will be compared against some simple approaches to the problem, which in occasions are adequate to set approximate bounds to the mismatch uncertainty. Its use is validated through comparison against the statistical simulations by MC or against the analytic solution in case it can be found in the literature.

3. Direct comparison transfer with two and three sensors

The direct comparison calibration of a power sensor is based on the comparison against a known reference or calibrated power sensor (Ref), i.e. whose calibration factor is known. The power splitter, used to divide the generated RF signal between the two sensors (in the two-sensor configuration, see Fig. 4) makes it possible to perform simultaneous measurement of power in the sensor under test (DUT) and in the calibrated standard sensor (Ref). In this way, and having previously characterized the devices involved (calibration factor of the standard sensor, and equivalent source match and tracking of the power splitter), the calibration factor of the DUT can be calculated. Furthermore, knowing all complex reflection coefficients in magnitude and phase, it is possible to correct the measured calibration factor for impedance mismatch.

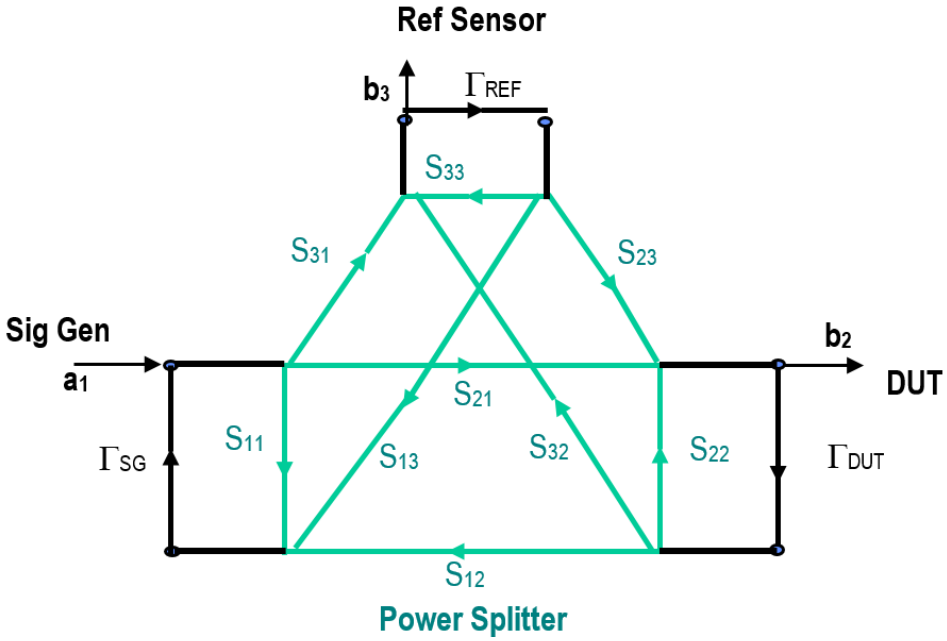

Fig. 4. Measurement setup for two-sensor configuration (Ref. [3] Ken Wong, Keysight Technologies)

The calibration factor (**CF**) of each sensor provides a relationship between the measured power (**M**) and the incoming signal **b** that reaches the sensor: **CF** = **M** / $|\mathbf{b}|^2$. In this case, the calibration factor of the sensor under test can be calculated from the relationship between signals $\mathbf{b_2}$ and $\mathbf{b_3}$ present at the output ports of the power splitter, and from the readings of both sensors:

$$CF_{DUT} = CF_{Ref} \cdot \frac{M_{DUT}}{M_{Ref}} \cdot \frac{|b_3|^2}{|b_2|^2} = CF_{Ref} \cdot \frac{M_{DUT}}{M_{Ref}} \cdot \frac{|S_{31}|^2}{|S_{21}|^2} \cdot \left| \frac{1 - \Gamma_{DUT} \cdot \Gamma_{Eq2}}{1 - \Gamma_{Ref} \cdot \Gamma_{Eq3}} \right|^2$$

This equation is dependent on the transmission [S] parameters of the power splitter (or just its difference, asymmetry or tracking between arms), as well as on the equivalent source match in both splitter outputs:

$$\Gamma_{Eq3} = S_{33} - \frac{S_{31} \cdot S_{32}}{S_{21}} \qquad \Gamma_{Eq2} = S_{22} - \frac{S_{21} \cdot S_{32}}{S_{31}}$$

The above configuration presents the disadvantage of being very sensitive to the accuracy with which the asymmetry of the splitter is known. The three-sensor configuration

avoids this unwanted dependence on the tracking between arms of the power splitter, see Fig. 5. The measurement procedure in this case consists in making two successive measurements using a similar setup. First, the leveling sensor (Ref) and a third standard sensor or traveling standard (Std) with a known calibration factor are connected to both arms of the power splitter, same configuration as before with standard sensor in place of DUT. Subsequently, the standard sensor is replaced by the sensor under test. Taking a look at the measurements made with the standard sensor, first connection, the tracking between arms of the power splitter can solved for as:

$$\frac{|S_{31}|^2}{|S_{21}|^2} = \frac{CF_{Std}}{CF_{Ref}} \cdot \frac{M_{Ref}}{M_{Std}} \cdot \left| \frac{1 - \Gamma_{Ref} \cdot \Gamma_{Eq3}}{1 - \Gamma_{Std} \cdot \Gamma_{Eq2}} \right|^2$$

Introducing this in the expression for the calibration factor of DUT eliminates the dependence on tracking. Eventually $\mathbf{CF_{DUT}}$ using the three-sensor configuration is given by:

$$CF_{DUT} = CF_{Std} \cdot \frac{M_{DUT}}{M_{Ref(DUT)}} \cdot \frac{M_{Ref(Std)}}{M_{Std}} \cdot \left| \frac{1 - \Gamma_{DUT} \cdot \Gamma_{Eq2}}{1 - \Gamma_{Std} \cdot \Gamma_{Eq2}} \right|^2$$

$\mathbf{M_{Ref(Std)}}$ is the indicated power at the monitoring (leveling) power sensor when the standard sensor is connected to Port 2, while $\mathbf{M_{Ref(DUT)}}$ is the indicated power at the monitoring sensor when the DUT sensor is connected to Port 2 of the power splitter. As can be seen, it is no longer necessary to know the asymmetry or tracking term, which eliminates the sensitivity of the method with respect to the measurement of attenuation in both arms of the splitter.

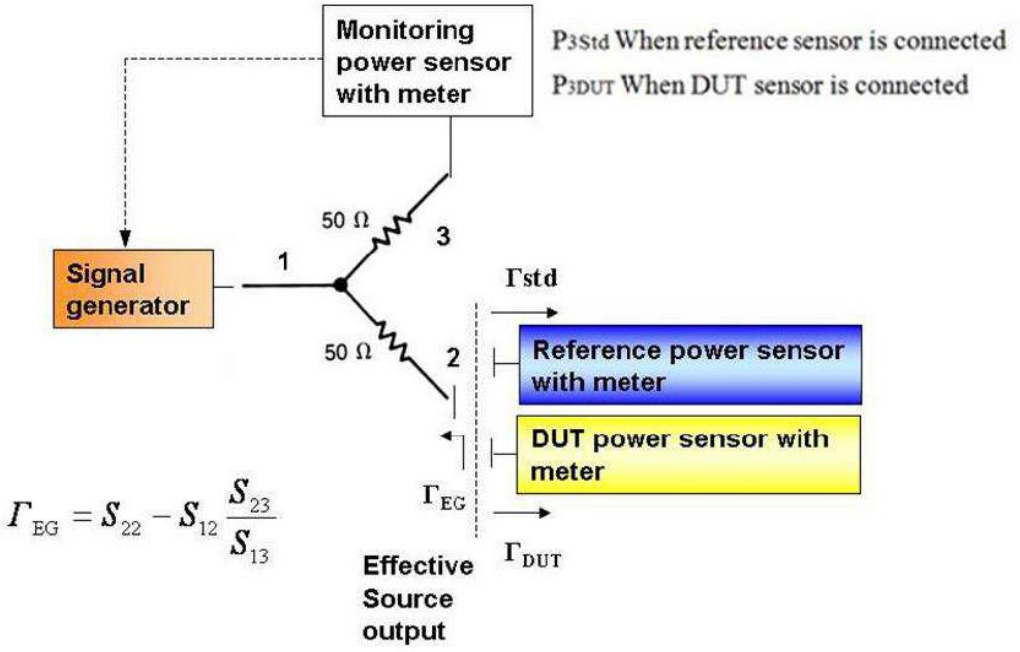

Fig. 5. Three-sensor configuration (Ref. [4] Yueyan Shan and Xiaohai Cui)

This equation only depends on the measurements taken by the three sensors and on a scalar correction term (dependent on complex quantities, though) which accounts for impedance mismatch. This mismatch effect is related to the complex reflection coefficients of the sensors and to the equivalent source match of the power splitter in one of its output ports. What is most important, this correction term can be determined because all involved reflection coefficients are known in magnitude and phase. It is important to stress that it is not always possible to perform this mismatch correction with other methods. For example using a temperature-stabilized feedthrough mount it is difficult to know the phase of the equivalent source match of the working standard.

As regards computation of **CF** uncertainty, it is no longer necessary to set bounds to the uncertainty associated with this mismatch contribution, in the form of a maximum value such as $200 \cdot |\boldsymbol{\Gamma}_{\mathbf{Std}}| \cdot |\boldsymbol{\Gamma}_{\mathbf{DUT}}|$ in percent. Instead, it is possible to compute it and to correct for it, in other words it becomes part of the mathematical model which gives us the calibration factor of the DUT. Thus its influence in the corrected **CF** is computed applying the Law of Propagation of Uncertainties (LPU) onto the mismatch correction term. In order to determine the sensitivity coefficients of each independent variable involved, it would be necessary to calculate the partial derivatives of the (scalar) correction term with respect to each complex variable, in its real and imaginary parts. This calculation is not simple, see Ref. [4]. A simplification consists in assuming that the independent variables are all scalar quantities, by doing this the mismatch uncertainty would be as follows:

$$U_M = 100 \cdot \left(\frac{2U_{\Gamma(DUT)}|\Gamma_{Eq2}| + 2U_{\Gamma(Eq2)}|\Gamma_{DUT}|}{|1 - \Gamma_{DUT} \cdot \Gamma_{Eq2}|} + \frac{2U_{\Gamma(Std)}|\Gamma_{Eq2}| + 2U_{\Gamma(Eq2)}|\Gamma_{Std}|}{|1 - \Gamma_{Std} \cdot \Gamma_{Eq2}|} \right) \; Worst\ case$$

$$U_M = 100 \cdot \sqrt{\frac{4U^2_{\Gamma(DUT)}|\Gamma_{Eq2}|^2 + 4U^2_{\Gamma(Eq2)}|\Gamma_{DUT}|^2}{|1 - \Gamma_{DUT} \cdot \Gamma_{Eq2}|^2} + \frac{4U^2_{\Gamma(Std)}|\Gamma_{Eq2}|^2 + 4U^2_{\Gamma(Eq2)}|\Gamma_{Std}|^2}{|1 - \Gamma_{Std} \cdot \Gamma_{Eq2}|^2}} \; R.s.s.$$

If we had to partially derive the mathematical model with respect to the real and imaginary parts of each variable, it would result in a cumbersome analytical calculation with many variables involved. To avoid this, we will make use of a numerical method such as Monte Carlo.

3.1 Uncertainty propagation using Monte Carlo

The MC method consists in simulating a sufficiently high number of realizations of the input variables to the mathematical model of the mismatch correction (in complex format, and taking their nominal value and associated uncertainty as starting point), and in combining them according to the equation so that eventually the histogram of possible values, or occurrences for the output variable can be computed (Fig. 6).

From the output variable, in our case the mismatch correction, it is possible to determine the expected value, the probability density function (p.d.f.) and the uncertainty interval for a given probability or level of confidence **p**.

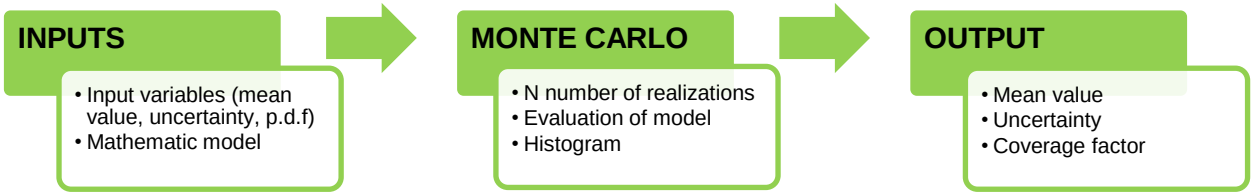

Fig. 6. The Monte Carlo method

Main advantages of the method are: (i) it is always valid, even if the central limit theorem is not applicable[1]; (ii) it allows the analysis of any output probability density function resulting from the combination of any number of input quantities, even if the resulting p.d.f. is not symmetric (LPU assumes symmetry of all input and output variables); and (iii) it overcomes the analytical difficulties related to partial differentiation.

The complex independent variables which are input to the MC method are, for the three-sensor configuration, the three reflection coefficients $\boldsymbol{\Gamma}_{\mathbf{DUT}}$, $\boldsymbol{\Gamma}_{\mathbf{Std}}$ and $\boldsymbol{\Gamma}_{\mathbf{Eq2}}$ which are known in terms of magnitude (and associated uncertainty) and phase, the uncertainty of phase being usually a function of the ratio between magnitude and its uncertainty. Using Monte Carlo,

[1] In general the GUM assumes a sufficiently high number of uncorrelated input variables so that the central limit theorem is applicable.

each reflection coefficient is simulated as two random variables, statistically independent and uncorrelated: the real and imaginary parts $\boldsymbol{\Gamma} = \boldsymbol{\Gamma}_r + \mathbf{j}\cdot\boldsymbol{\Gamma}_i$. Each complex variable is simulated by a Gaussian probability density function (p.d.f.) with zero correlation coefficient and variances $u^2(\boldsymbol{\Gamma}_r)$, $u^2(\boldsymbol{\Gamma}_i)$. The resulting p.d.f. in two dimensions is called bivariate Gaussian.

The previous characterization of every involved reflection coefficient provides knowledge about its magnitude $|\boldsymbol{\Gamma}|$ and associated uncertainty $u(|\boldsymbol{\Gamma}|)$ and also about its phase $\angle\boldsymbol{\Gamma}$. In order to generate random values for the input variables, usual assumption is to take the real and imaginary parts as independent and uncorrelated, both with the same uncertainty: e.g. $\boldsymbol{\Gamma}_r \pm u(|\boldsymbol{\Gamma}|)$, $\boldsymbol{\Gamma}_i \pm u(|\boldsymbol{\Gamma}|)$.

We have applied MC to a case study with measured values for reflection coefficient (DUT and power splitter measured in INTA) and making use of an external calibration certificate (standard sensor). With N = 10000 simulations, the cloud of complex values for the input random variables shown in Fig. 7 for a single frequency is obtained. In a general case there would be a correlation between the real and imaginary parts (we would be observing ellipses instead of circles of uncertainty), but in this guide we will ignore correlation: in general it would make the clouds more flattened, resembling an ellipse with a certain angle of inclination.

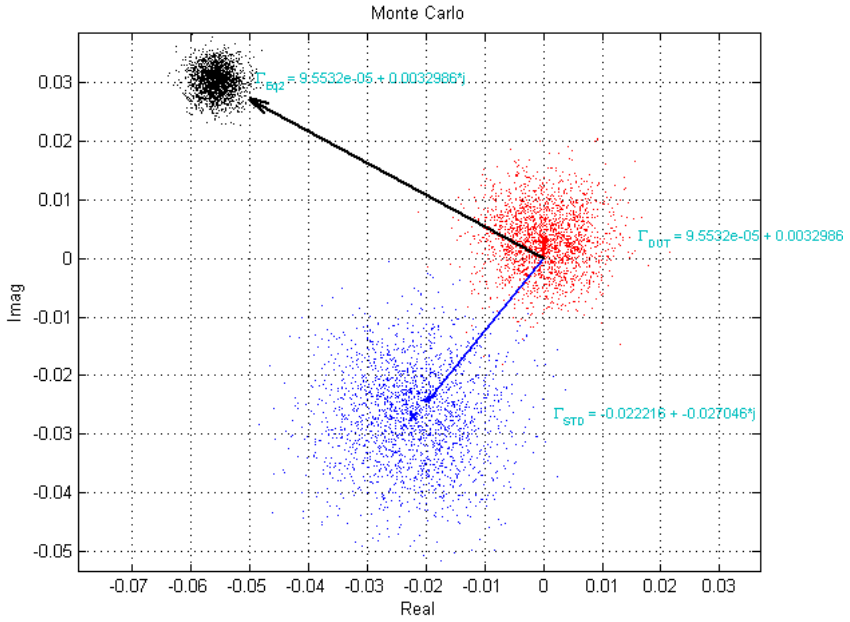

Fig. 7. Monte Carlo simulation of the complex reflection coefficients of DUT, standard and splitter

For each input vector, we have simulated N realizations, of which approximately 95% are comprised within a circle centered on $\boldsymbol{\Gamma} = \boldsymbol{\Gamma}_r + \mathbf{j}\cdot\boldsymbol{\Gamma}_i$ and with radius $u(|\boldsymbol{\Gamma}|)$. The coverage factor $\mathbf{k}$ = 2 in a one-dimensional Gaussian distribution corresponds to a probability $\mathbf{p}$ = 0.9545, while for a bivariate Gaussian the coverage factor to be considered is $\mathbf{k}$ = 2.45 for a probability or level of confidence $\mathbf{p}$ = 0.95. However, in our case it is not necessary to analyze uncertainty regions in two dimensions, since we are only interested in a scalar correction (the output variable of the mathematical model, i.e. the mismatch correction is one-dimensional). Just for illustrative purposes, see Fig. 8 for a complex representation of the mismatch correction before taking the modulus squared.

The modulus of the mismatch correction exhibits a histogram that converges approximately to a Gaussian p.d.f. in one dimension, see Fig. 9. The average value coincides with the nominal value of the correction:

$$Mismatch\ correction = \left|\frac{1-\Gamma_{DUT}\cdot\Gamma_{Eq2}}{1-\Gamma_{Std}\cdot\Gamma_{Eq2}}\right|^2$$

The uncertainty associated to the mismatch correction for a probability **p** = 0.9545, is computed as the range of values of the output variable that encompasses 95.45% of the histogram occurrences. However, the resulting distribution obtained by MC is not completely symmetric, see Fig. 9.

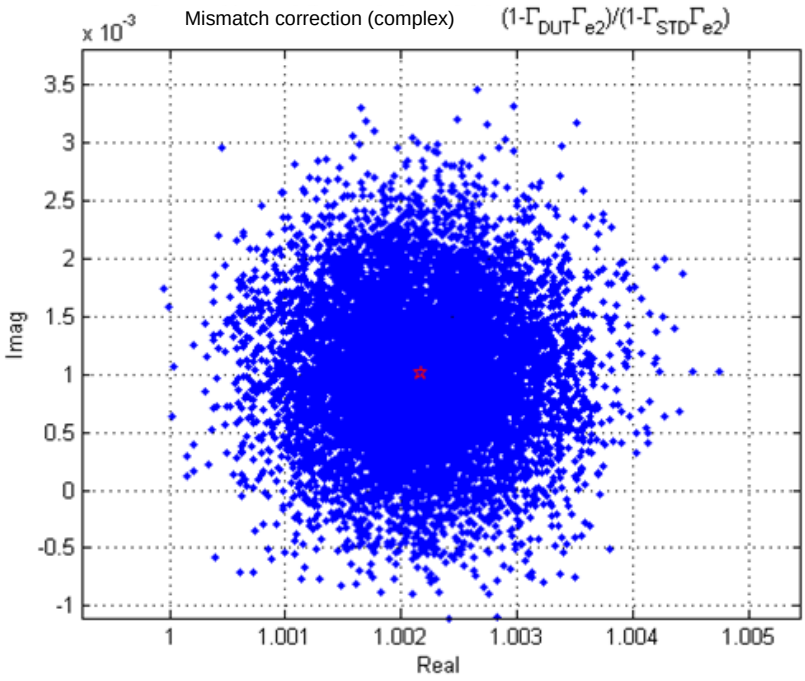

Fig. 8. Complex mismatch correction, from which the square of the modulus is computed

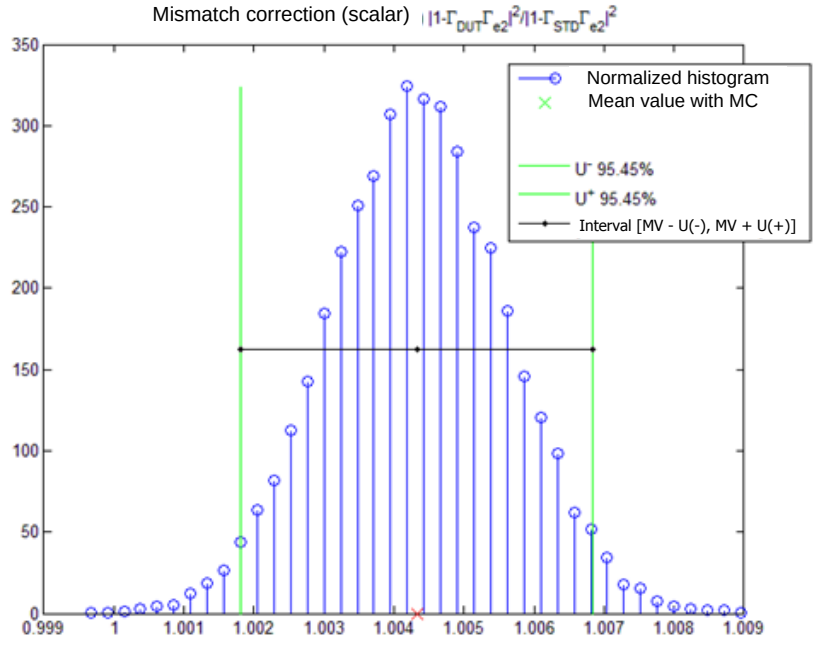

Fig. 9. Histogram of the mismatch correction term (scalar)

According to the 'Guide to the Expression of Uncertainty in Measurement' (GUM, Ref. [1]), in these cases the uncertainty interval to be considered is the minimum amplitude that includes the stated percentage of probability, i.e. it is defined by the average value and a two uncertainty values (higher and lower):

$$[\bar{x} - U^{-}, \bar{x} + U^{+}]$$

3.2 Comparison between MC and the LPU

The Monte Carlo method has been applied to the direct comparison calibration of a power sensor using the three-sensor configuration. Connector type was PC 3.5 mm and the measurement range 19 GHz to 26.5 GHz in 1 GHz steps. The results have been compared with those obtained applying partial differentiation to the mathematical model according to the LPU. MC results have also been compared against the maximum bound computed for the mismatch correction in those cases in which it is not possible to apply corrections due to the lack of knowledge about the phase of the complex reflection coefficients involved. This maximum bound is given by the following scalar equation:

$$U(\%) \leq \sqrt{\left(200 \cdot |\Gamma_{DUT}| \cdot |\Gamma_{Eq2}|\right)^2 + \left(200 \cdot |\Gamma_{Std}| \cdot |\Gamma_{Eq2}|\right)^2}$$

The comparison can be seen in Tab. 1 and Fig. 10. For the sake of clarity, the maximum bound is shown in the form of error bars superimposed onto the nominal value of the mismatch correction.

Frequency (GHz)	Monte Carlo method			Law of Propagation of Uncertainties (LPU)		Maximum Bound
	Correction	U- (%)	U+ (%)	Correction	U (%)	U (%)
19	1.004336	0.002434	0.002529	1.004334	0.002487	0.004454
20	1.002373	0.002462	0.002538	1.002372	0.002509	0.005711
21	0.996440	0.001959	0.001880	0.996440	0.001904	0.004747
22	1.000844	0.001739	0.001721	1.000845	0.001704	0.004458
23	0.998734	0.001771	0.001781	0.998734	0.001764	0.004399
24	1.000018	0.001475	0.001438	1.000017	0.001442	0.002851
25	1.003740	0.001907	0.001904	1.003740	0.001914	0.004554
26	0.991506	0.002393	0.002446	0.991506	0.002427	0.007338
26.5	0.989514	0.002436	0.002478	0.989513	0.002454	0.007791

Tab. 1. Comparison among MC method, LPU and maximum bound for mismatch (no correction)

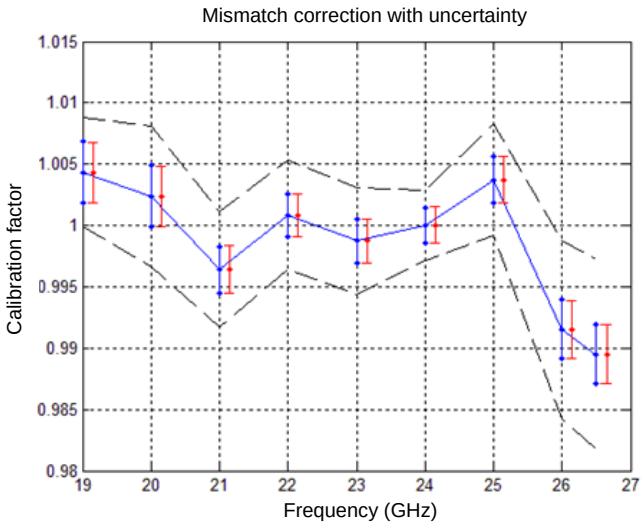

Fig. 10. Mismatch correction (Blue: MC method / Red: LPU / Black: maximum bound)

3.3 Correction for the [S] parameters of a padding attenuator or adapter

In some cases, adapters are used at the output of the power splitter because the connector type of the standard sensor does not match that of the unit under test (traceable, calibrated sensors are not always available for all connector types).

When performing a calibration of power sensor for low-power (diode type sensor), and assuming that we do not have a calibrated low-power diode type sensor, which would double our periodic investment in external calibrations, it is necessary to reduce the incident power in a diode by means of a padding attenuator.

In both cases, the adapter / attenuator used at the output of the splitter must be previously characterized in terms of [S] parameters in magnitude and phase, in order to correct the measured calibration factor of the sensor under test. This can be regarded also as 'de-embedding' the diode.

Note that, since our correction method is complex in its definition (although we finally correct the measured **CF** just by the modulus of a complex quantity) all four [S] parameters have to be known in magnitude and phase. The traditional approach making use of a temperature-stabilized feedthrough mount, scalar by definition, only requires scalar characterization of the adapter / attenuator used (i.e. magnitude of $\mathbf{S_{21}}$ in dB). In this case, since we do not correct for mismatch, the information about magnitude of the reflection coefficients $\mathbf{S_{11}}$ and $\mathbf{S_{22}}$ of the attenuator are incorporated into the worst-case mismatch uncertainty in the form of a maximum bound (two connection planes have to be considered, between feedthrough and attenuator and between attenuator and DUT).

See Fig. 11. The attenuator is placed between the output port of the power splitter and the device under test (DUT). With a 30 dB padding attenuator, the power reaching the DUT is in the order of the microwatts (instead of milliwatts at the output of the splitter).

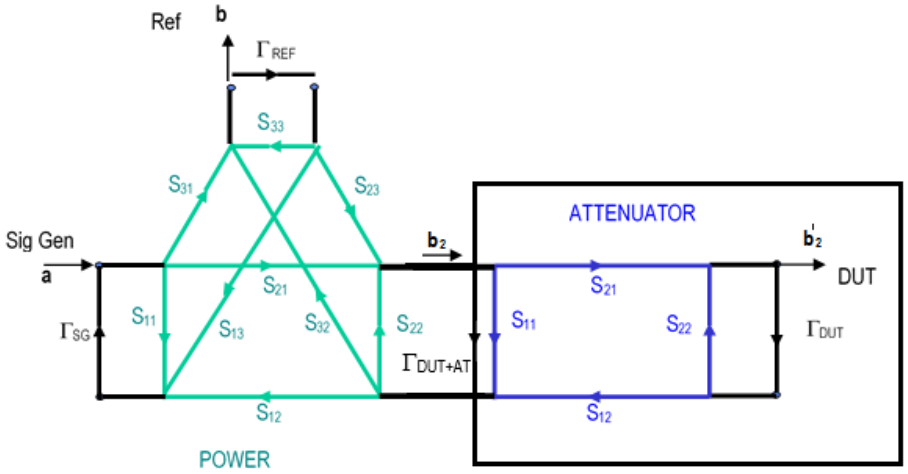

Fig. 11. Measurement setup with padding attenuator (Ref. [3] Ken Wong, Keysight Technologies).

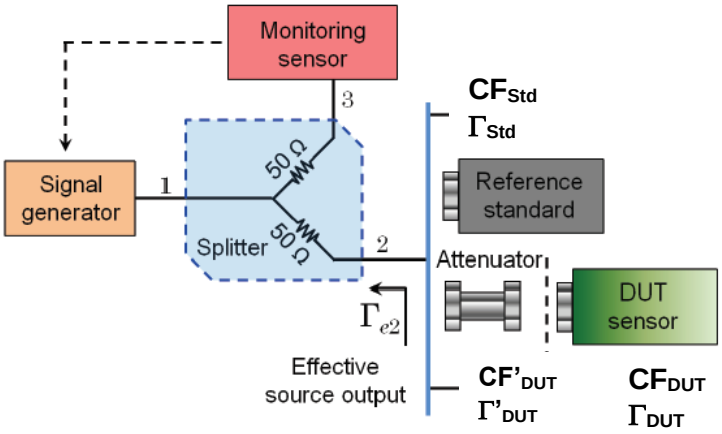

Fig. 12. Measurement setup with signals involved (Ref. [5] Yu Song Meng and Yueyan Shan)

In addition to having the power splitter and the two power sensors characterized in terms of complex reflection coefficient (**Γ_{Eq2}**, **Γ_{DUT}** and **Γ_{Std}**), it is necessary to know the attenuator's [S] parameters in magnitude and phase. This allows us to transfer the DUT's reflection coefficient to the input plane of attenuator[2] **Γ'_{DUT}**, as well as the measured power at DUT, for which some mathematics is needed.

We will use the well-known formula for the insertion loss as a function of the [S] parameters of a two-port device and of the reflection coefficients of generator and load (looking to the left at the input of the device, Γ_{Eq2} in our terminology, and to the right at the output of the device, that is Γ_{DUT}). This formula in a similar notation can be found in Warner Ref [6]:

$$IL(dB) = 20 \cdot log_{10} \frac{\left|\left(1 - S_{11} \cdot \Gamma_{Eq2}\right) \cdot \left(1 - S_{22} \cdot \Gamma_{DUT}\right) - S_{12} \cdot S_{21} \cdot \Gamma_{Eq2} \cdot \Gamma_{DUT}\right|}{|S_{21}|}$$

Attenuation being:

$$A(dB) = 20 \cdot log_{10} \frac{1}{|S_{21}|}$$

The measured power at the input of the sensor under test **M_{DUT}** must be corrected by the above expression for insertion loss in linear terms, in order to obtain the signal present at the output port of the power splitter, i.e. input to the attenuator. It is this signal which has to be known at the input of the attenuator, and not what the detected power at the DUT would be if connected directly to the power splitter (this is the reason why we are not using the traditional expression for insertion loss!):

$$M'_{DUT} = M_{DUT} \cdot \frac{\left|\left(1 - S_{11} \cdot \Gamma_{Eq2}\right) \cdot \left(1 - S_{22} \cdot \Gamma_{DUT}\right) - S_{12} \cdot S_{21} \cdot \Gamma_{Eq2} \cdot \Gamma_{DUT}\right|^2}{|S_{21}|^2}$$

Or, rearranging terms in the numerator, see Ref. [7]:

$$M'_{DUT} = M_{DUT} \cdot \frac{|1 - S_{22} \cdot \Gamma_{DUT}|^2 \cdot \left|1 - \Gamma'_{DUT} \cdot \Gamma_{Eq2}\right|^2}{|S_{21}|^2}$$

$$\Gamma'_{DUT} = S_{11} + \frac{S_{12} \cdot S_{21} \cdot \Gamma_{DUT}}{1 - S_{22} \cdot \Gamma_{DUT}}$$

Note the difference between **Γ'_{DUT}** and **$\Gamma_{A\text{-}DUT}$** used in other reference articles. Now, knowing how to correct the measurements made with the sensor under test, 'moving' between reference planes, it is possible to obtain a unique formula for the DUT's calibration factor. **CF_{DUT}** depends on the four measurements made with the three sensors involved, as well as on two correction terms: the one shown in grey can be seen as the same mismatch correction for the connection of the standard as in the case of 'no-padding', whereas the terms coloured in pink account for the overall effect of the attenuator used between splitter and sensor, and represent the power **M'_{DUT}** that would be measured at the input of the attenuator:

$$CF_{DUT} = CF_{Std} \cdot \frac{M'_{DUT}}{M_{Ref(DUT)}} \cdot \frac{M_{Ref(Std)}}{M_{Std}} \cdot \frac{1}{\left|1 - \Gamma_{Std}\Gamma_{Eq2}\right|^2} = \cdots$$

$$\cdots = CF_{Std} \cdot \frac{M_{DUT}}{M_{Ref(DUT)}} \cdot \frac{M_{Ref(Std)}}{M_{Std}} \cdot \frac{|1 - S_{22} \cdot \Gamma_{DUT}|^2 \cdot \left|1 - \Gamma'_{DUT} \cdot \Gamma_{Eq2}\right|^2}{|S_{21}|^2} \cdot \frac{1}{\left|1 - \Gamma_{Std}\Gamma_{Eq2}\right|^2}$$

$$\Gamma'_{DUT} = S_{11} + \frac{S_{12} \cdot S_{21} \cdot \Gamma_{DUT}}{1 - S_{22} \cdot \Gamma_{DUT}}$$

[2] It is also possible to measure the set of 'attenuator + DUT sensor', see approximate formula. However, the whole mathematic approach described here allows us to account for this change in the reference plane of the different reflection coefficients involved.

It can be seen that, making $\mathbf{S_{11}}$ = $\mathbf{S_{22}}$ = 0, $\mathbf{S_{21}}$ = $\mathbf{S_{12}}$ = 1, that is the case where no attenuator exists, the formula reduces to the expression seen for mid-power sensors in the three-sensor configuration, see Section 3 above.

All involved mismatches are taken into account: if examined carefully, it can be seen that two connection planes are considered, between the power splitter and the attenuator input, and between the attenuator output and the sensor under test. A simplification of the above formula consists in considering the set 'attenuator + sensor' the unit under test, thus accounting for mismatch at just one connection plane, and ignoring the complex [S] parameters of the attenuator, except for magnitude of $\mathbf{S_{21}}$ (shown in green below, necessary to correct for $\mathbf{M'_{DUT}}$). In this case, the reflection coefficient $\mathbf{\Gamma'_{DUT}}$ has to be measured or calculated:

$$CF_{DUT} \cong CF_{Std} \cdot \frac{M_{DUT}}{M_{Ref(DUT)}} \cdot \frac{M_{Ref(Std)}}{M_{Std}} \cdot \frac{1}{|S_{21}|^2} \cdot \left| \frac{1 - \Gamma'_{DUT} \cdot \Gamma_{Eq2}}{1 - \Gamma_{Std} \cdot \Gamma_{Eq2}} \right|^2$$

$$\Gamma'_{DUT}: measured$$

Again we will apply the Monte Carlo method to determine the uncertainty interval associated to both corrections. This method has been applied to the direct comparison calibration of a Hewlett Packard 8487D diode sensor fitted with PC 2.4 mm connector, using the three-sensor configuration and making use of a 20 dB padding attenuator. The correction term for the attenuator has a value around 100 which is its approximate linear insertion loss. Uncertainties have been computed for a probability or level of confidence **p** = 0.9545, equivalent to a coverage factor **k** = 2 in the case of a one-dimensional Gaussian distribution. Applying partial derivatives to the mathematic model according to the LPU leads to the same results as those obtained with Monte Carlo.

The results are shown in Tab. 2 and Tab. 3. Fig. 13 shows all possible corrections to be applied, including the different contributions (shown in pink, grey and green) which add up to the overall mismatch correction and to the simplified formula.

Note that the error bars in Fig. 14 include not only the mismatch contribution, but also additional contributions such as **CF** of the standard sensor, drift, power meter accuracy and repeatability.

As can be seen in the graphical representation, the results and their uncertainty are compatible with the values originally included by the manufacturer in the table attached to the sensor body, even though these are the original factory values and have never been re-tested by the manufacturer. Our approach shows also the results obtained with the simplified formula for $\mathbf{CF_{DUT}}$ and without mismatch correction (applying only $\mathbf{S_{21}}$ correction).

Frequency (GHz)	Monte Carlo method			Law of Propagation of Uncertainties (LPU)	
	Correction	U- (%)	U+ (%)	Correction	U (%)
0.1	89.905	0.480	0.486	89.905	0.466
0.5	90.089	0.413	0.393	90.089	0.392
1	90.203	0.355	0.373	90.203	0.361
2	90.412	0.361	0.366	90.412	0.360
3	90.647	0.380	0.369	90.647	0.368
4	90.913	0.390	0.369	90.913	0.371
5	91.205	0.385	0.372	91.205	0.374
6	91.557	0.397	0.387	91.557	0.385
7	91.939	0.408	0.402	91.939	0.400
8	92.326	0.412	0.432	92.325	0.411
9	92.690	0.427	0.438	92.690	0.427
10	93.150	0.462	0.459	93.149	0.452
11	93.791	0.498	0.476	93.790	0.479
12	94.465	0.515	0.500	94.465	0.502
13	94.923	0.561	0.528	94.923	0.534
14	95.324	0.553	0.596	95.324	0.570
15	96.121	0.611	0.614	96.121	0.606
16	97.620	0.632	0.611	97.619	0.614
17	98.725	0.595	0.626	98.724	0.611
18	99.011	0.613	0.662	99.010	0.632
19	99.346	0.580	0.604	99.346	0.587
20	100.651	0.618	0.609	100.650	0.598
21	102.147	0.709	0.744	102.146	0.711
22	102.649	0.795	0.757	102.648	0.762
23	102.915	0.824	0.796	102.914	0.801
24	104.831	0.816	0.792	104.830	0.781
25	107.169	0.709	0.795	107.168	0.729
26	108.218	0.657	0.684	108.216	0.660
27	108.425	0.599	0.596	108.425	0.589
28	109.924	0.768	0.736	109.923	0.725
29	111.441	0.966	0.957	111.439	0.935
30	112.148	1.062	1.052	112.146	1.052
31	112.843	1.091	1.067	112.840	1.068
32	114.930	1.028	1.022	114.929	1.002
33	116.678	0.984	1.074	116.677	1.013
34	118.354	1.072	1.126	118.353	1.084
35	120.085	1.133	1.216	120.083	1.170
36	119.150	1.333	1.312	119.148	1.320
37	117.510	1.630	1.524	117.506	1.568
38	120.811	1.732	1.722	120.807	1.719
39	127.034	1.620	1.649	127.031	1.624
40	127.047	1.529	1.517	127.041	1.515

Tab. 2. Comparison among MC and LPU (diode sensor, 2.4 mm, 20 dB attenuator correction)

Frequency (GHz)	INTA			Manufacturer	Simplified	S21 only
	CF_{DUT}	U- (%)	U+ (%)	CF_{DUT}	CF_{DUT}	CF_{DUT}
0.1	0.944	1.2	1.2		0.944	0.944
0.5	0.940	1.1	1.1		0.940	0.940
1	0.9395	1.0	1.0		0.9395	0.9396
2	0.9421	1.0	1.0	0.943	0.9421	0.9421
3	0.9377	1.0	1.0		0.9377	0.9377
4	0.9348	1.0	1.0		0.9349	0.9348
5	0.934	1.1	1.1		0.934	0.933
6	0.932	1.1	1.1		0.932	0.931
7	0.934	1.1	1.1		0.933	0.933
8	0.931	1.1	1.1		0.931	0.931
9	0.933	1.2	1.2		0.933	0.934
10	0.929	1.2	1.2	0.936	0.930	0.930
11	0.931	1.2	1.2		0.931	0.931
12	0.936	1.2	1.2		0.936	0.936
13	0.931	1.3	1.2		0.932	0.932
14	0.927	1.3	1.3	0.941	0.930	0.931
15	0.933	1.3	1.3		0.934	0.936
16	0.934	1.4	1.4		0.928	0.930
17	0.941	1.4	1.4		0.935	0.935
18	0.928	1.4	1.4	0.934	0.930	0.927
19	0.923	1.9	1.9		0.928	0.927
20	0.927	1.9	1.9	0.929	0.927	0.928
21	0.930	1.9	2.0		0.926	0.926
22	0.936	2.0	1.9	0.955	0.937	0.937
23	0.939	2.0	2.0		0.944	0.948
24	0.949	2.0	2.0	0.952	0.948	0.951
25	0.952	2.0	2.0		0.949	0.944
26	0.953	2.0	2.0	0.966	0.952	0.946
27	0.959	2.2	2.2		0.957	0.961
28	0.961	2.2	2.2	0.96	0.956	0.961
29	0.964	2.3	2.3		0.970	0.963
30	0.961	2.3	2.3	0.979	0.975	0.964
31	0.973	2.4	2.3		0.970	0.981
32	0.986	2.4	2.4	0.986	0.978	0.987
33	0.978	2.4	2.4		0.987	0.976
34	0.982	2.3	2.3	0.993	0.988	0.976
35	1.005	2.8	2.8		0.982	0.995
36	0.993	2.5	2.5	0.997	0.985	1.000
37	0.947	2.6	2.6		0.989	0.978
38	0.963	2.7	2.7	0.992	0.995	0.976
39	1.019	2.7	2.7		0.986	0.991
40	1.001	2.6	2.5	0.983	0.967	0.980

Tab. 3. Measurement results of a HP 8487D diode sensor fitted with PC 2.4 mm

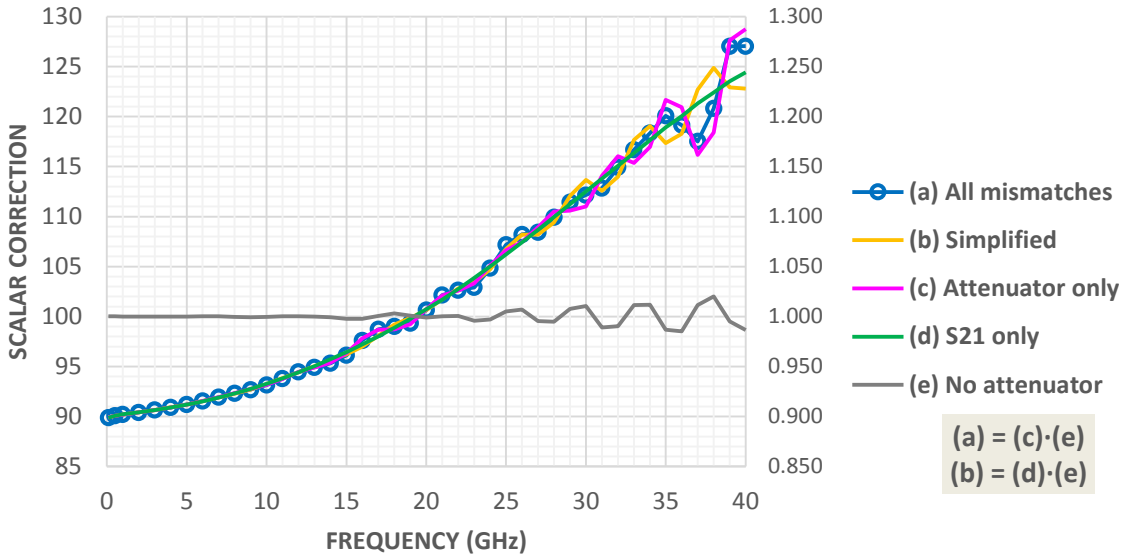

Fig. 13. All possible corrections (for No attenuator, look at right-hand Y-axis)

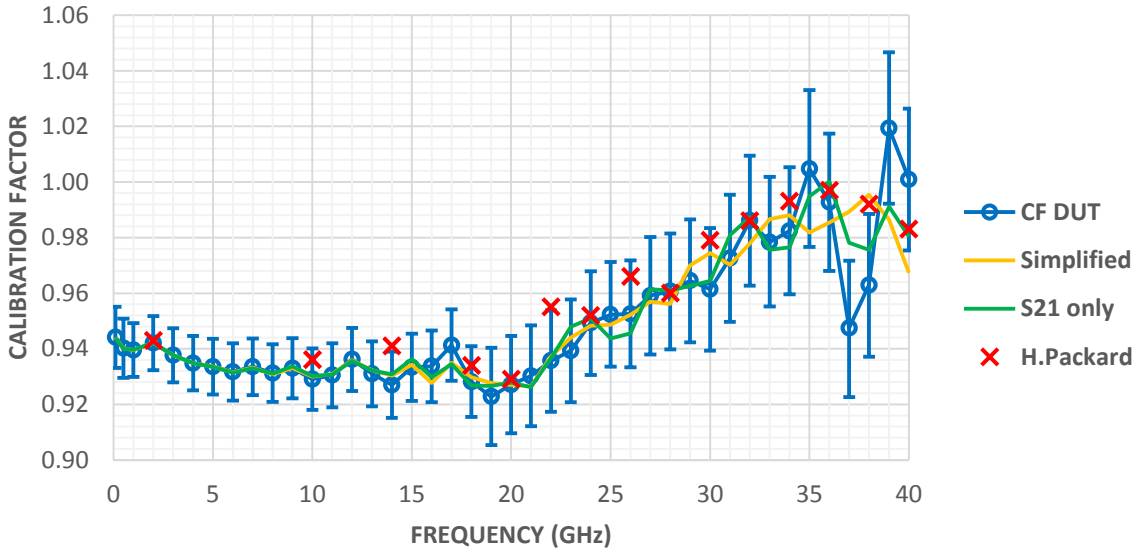

Fig. 14. Graphical representation of measured CF

4. Conclusions

The direct comparison transfer for calibration of power sensors has the advantage that it does not require high-cost instrumentation as it is the case for temperature-stabilized thermistor mounts. In addition, it allows impedance mismatch correction since all reflection coefficients are known in magnitude and phase.

However, the analytical calculation of the uncertainty associated with mismatch correction implies partial differentiation of complex (cumbersome) expressions which are dependent on a number of variables in real and imaginary parts. As an alternative, use of the Monte Carlo method has been proposed: it allows computation of the uncertainty intervals associated with the mismatch correction for a probability or level of confidence **p** = 0.9545.

As one of its main advantages, Monte Carlo allows propagation of probability density functions through any mathematical model, even if the central limit theorem (CLT) is not valid and the output variable is not symmetric (Gaussian of Student's t). GUM and LPU assume the CLT and symmetry in the input and output random variables.

Eventually, a higher and a lower uncertainty budget is provided, corresponding to the minimum amplitude interval that encompasses 95.45% of the occurrences of the output histogram. The results obtained by MC have been validated comparing them against the expanded uncertainty (**k** = 2) obtained by the analytical calculation (LPU).

The simplicity of the setup allows calibration of sensors in a wide range of working frequencies and for different types of connectors, simply using adapters (to change the connector type) or attenuators (to reduce the power reaching low-power diode sensors). In this way, it is not necessary to purchase and characterize additional standard sensors. An example has been presented of use of a padding 20 dB attenuator for calibration of a diode sensor with traceability to a thermocouple sensor in the milliwatt range, where the calibration factor of the diode under test must be corrected for an additional term due to the attenuator used. The formula and its simplified version for mismatch correction have been presented, as a function of the reflection coefficients involved and of the attenuator's [S] parameters. Monte Carlo allows computation of uncertainty associated to the overall correction, which adds directly to the uncertainty of **CF**.

Finally, a further reduction of uncertainties can be achieved if the miscellaneous instrumentation (power splitter and padding attenuator) are treated as traveling standards whose correction factors provide traceability to the method. Every refinement in the knowledge of equivalent source match of the splitter, and of the complex [S] parameters of the attenuator, for example sending them for external calibration together with the standard sensor, reduces the uncertainty of the direct comparison transfer method.

5. Acknowledgement

This work was supported by the project 15RPT01 RFMicrowave. This project has received funding from the EMPIR programme co-financed by the Participating States and from the European Union's Horizon 2020 research and innovation programme.

6. References

[1] *Evaluation of mesurement data – Guide to the Expression of Uncertainty in Measurement (GUM)*. Joint Committee for Guides in Metrology

[2] *Evaluation of mesurement data – Supplement 1 to the 'Guide to the Expression of Uncertainty in Measurement (GUM)' – Propagation of distributions using a Monte Carlo method*. Joint Committee for Guides in Metrology

[3] Ken Wong. *Power Sensor Cal Factor (Test Support Document)*. Keysight Technologies

[4] Yueyan Shan and Xiaohai Cui. *RF and Microwave Power Sensor Calibration by Direct Comparison Transfer*. Modern Metrology Concerns, Dr. Luigi Cocco (Ed.), ISBN: 978-953-51-0584-8, InTech, Available: http://www.intechopen.com/books/modern-metrology-concerns/rf-and-microwave-power-sensorcalibration-by-direct-comparison-transfer

[5] Yu Song Meng and Yueyan Shan. *Measurement and Calibration of a High-Sensivity Microwave Power Sensor with an Attenuator*. Radioengineering, Vol. 23, No. 4, Dec. 2014

[6] F L Warner. *Microwave Attenuation Measurement*. 1997, Peter Peregrinus Ltd. Chapter 2.9

[7] C Chirgwin, T P Crowley, W Fang and D LeGolvan. *Comparison of Power Ratio and Vector Network Analyzer Techniques for Measuring Attenuation*. 80th ARFTG Microwave Measurement Conference, November 2012. DOI: 10.1109/ARFTG.2012.6422438. Available: https://ieeexplore.ieee.org/document/6422438

[8] P Rakonjac et al. *Automated Power Sensors Calibration up to 26.5*. Mikrotalasna revija, December 2008

[9] *Coaxial RF Power Standard Instruction and Service Manual*. PN#IM300, April 2015. Available at: www.tegam.com